European Coordination for Accelerator Research and Development

PUBLICATION

Prospects of warm dense matter research at HiRadMat facility at CERN using 440 MeV SPS proton beam

Tahir, N A (GSI) *et al*

05 June 2013

The research leading to these results has received funding from the European Commission under the FP7 Research Infrastructures project EuCARD, grant agreement no. 227579.

This work is part of EuCARD Work Package **8: Collimators & materials for higher beam power beam**.

The electronic version of this EuCARD Publication is available via the EuCARD web site <http://cern.ch/eucard> or on the CERN Document Server at the following URL : <http://cds.cern.ch/record/1553473

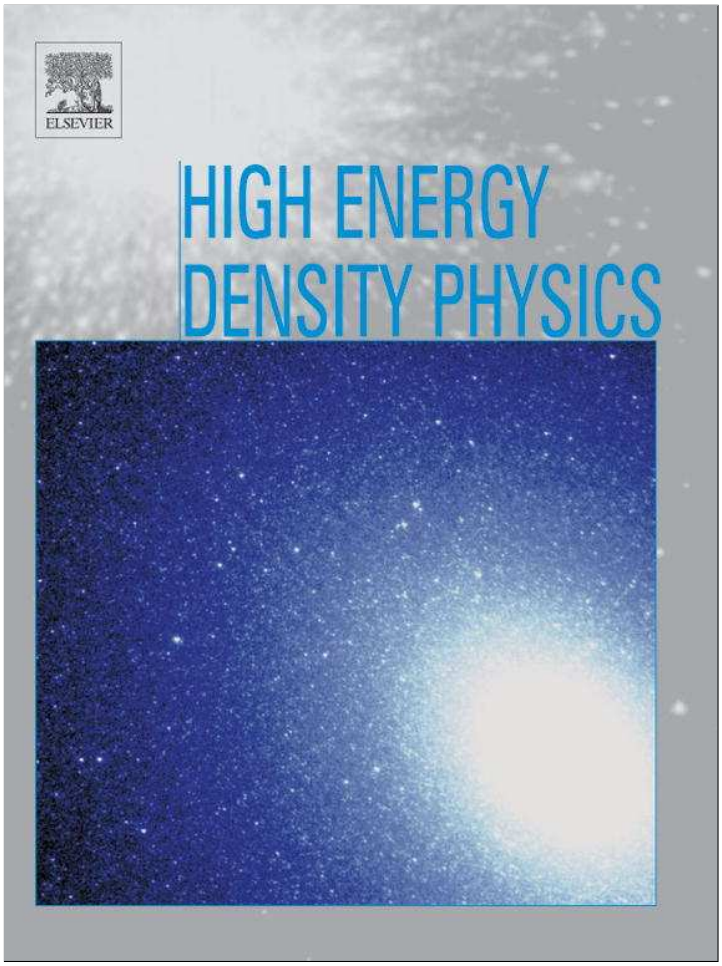

(This is a sample cover image for this issue. The actual cover is not yet available at this time.)

High Energy Density Physics 9 (2013) 269–276

Contents lists available at SciVerse ScienceDirect

High Energy Density Physics

journal homepage: www.elsevier.com/locate/hedp

Prospects of warm dense matter research at HiRadMat facility at CERN using 440 MeV SPS proton beam

N.A. Tahir [a,*], J. Blanco Sancho [b], R. Schmidt [c], A. Shutov [d], A.R. Piriz [e]

[a] GSI Helmholzzentrum für Schwerionenforschung, Planckstrasse 1, 64291 Darmstadt, Germany
[b] CERN-AB, 1211 Geneva 23, Switzerland and EPFL Lausanne, Switzerland
[c] CERN-AB, 1211 Geneva 23, Switzerland
[d] Institute of Problems of Chemical Physics, Russian Academy of Sciences, Institutskii pr. 18, 142432 Chernogolovka, Russia
[e] E.T.S.I. Industriales, Universidad de Castilla-La Mancha, 13071 Ciudad Real, Spain

ARTICLE INFO

Article history:
Received 28 November 2012
Received in revised form
22 December 2012
Accepted 25 December 2012
Available online 23 January 2013

Keywords:
Warm dense matter
Strongly coupled plasmas
High intensity proton beams

ABSTRACT

In this paper we present numerical simulations of heating of a solid copper cylinder by the 440 GeV proton beam delivered by the Super Proton Synchrotron (SPS) at CERN. The beam is made of 288 proton bunches while each bunch comprises of $1.15\cdot10^{11}$ so that the total number of protons in the beam is about $1.3\cdot10^{13}$. The bunch length is 0.5 ns while two neighboring bunches are separated by 25 ns so that the beam duration is 7.2 μs. Particle intensity distribution in the transverse direction is a Gaussian and the beam can be focused to a spot size with $\sigma = 0.1$ mm−1.0 mm. In this paper we present results using two values of σ, namely 0.2 mm and 0.5 mm, respectively. The target length is 1.5 m with a radius = 5 cm and is facially irradiated by the beam. The energy deposition code FLUKA and the two-dimensional hydrodynamic code BIG2 are employed using a suitable iteration time to simulate the hydrodynamic and the thermodynamic response of the target. The primary purpose of this work was to design fixed target experiments for the machine protection studies at the HiRadMat (High Radiation Materials) facility at CERN. However this work has shown that large samples of High Energy Density (HED) matter will be generated in such experiments which suggests an additional application of this facility. In the present paper we emphasize the possibility of doing HED physics experiments at the HiRadMat in the future.

1. Introduction

Due to their high efficiency and high repetition rate, ion beam drivers are a very attractive tool for inertial confinement fusion studies [1–10] as well as for the generation of High Energy Density (HED) matter in the laboratory [11–33]. It is to be noted that the Large Hadron Collider (LHC) at CERN is the most powerful accelerator in the world. The main purpose of this impressive machine is to research particle physics. However, extensive theoretical work based on sophisticated numerical simulations has been carried out over the past decade to study the damage caused by the full impact of one LHC beam on solid targets of different materials including copper and graphite [18,19,34,35]. These studies have shown that the range of the 7 TeV LHC protons is substantially increased in the target due to the so called "hydrodynamic tunneling" phenomenon. For example, in solid graphite, the protons and the shower can penetrate up to 25 m where as their range in a static approximation is about 4 m. Similar calculations have also been reported elsewhere [36]. Although, this work was done primarily within the framework of the machine protection system studies, and a very interesting outcome of this work was that the impact of the LHC protons on solid targets can generate huge samples of HED matter. This has been recognized as an additional, very important application of the LHC [19].

It is always desirable to have experimental verification of numerical simulations in order to be sure about the validity of the theoretical predictions. However it is not possible in case of the LHC. To overcome this problem, an experimental facility named HiRadMat (High Radiation Materials) has been established at CERN to conduct beam–target interaction experiments using the 440 GeV proton beam from the Super Proton Synchrotron (SPS). Detailed simulations of design studies of such experiments have systematically been done over the past years and are reported elsewhere [34,37–39]. Recently, experiments have been carried out

* Corresponding author. Tel.: +49 6159 71 2293; Fax: +49 6159 71 2992.
E-mail address: n.tahir@gsi.de (N.A. Tahir).

1574-1818/$ – see front matter © 2013 Elsevier B.V. All rights reserved.
http://dx.doi.org/10.1016/j.hedp.2012.12.010

at the HiRadMat facility using solid copper cylindrical targets to study the "hydrodynamic tunneling" phenomenon in case of the SPS protons. First analysis of these results indicates an agreement with the simulations [40]. However, to establish the correct degree of accuracy of the simulations in a quantitative manner, one has to wait until the detailed analysis of the experiments has been completed. The outcome of these studies will be published accordingly. In the present paper, we discuss the HED physics aspects of the most recent theoretical work, highlighting the possibility of doing HED physics experiments at the HiRadMat facility.

In Section 2 we describe the HiRadMat facility including the beam and the target parameters. The simulation results are presented in Section 3 while the conclusions drawn from this work are noted in Section 4.

2. HiRadMat test facility and the Super Proton Synchrotron

The Super Proton Synchrotron (SPS) is used as LHC injector, but also to accelerate and extract protons and ions (such as lead and other ion species) for fixed target experiments and for producing neutrinos (CNGS). In particular the risks during the fast extraction of LHC and CNGS beams must be considered since any failure during this process can lead to serious equipment damage.

The SPS accelerator is 6.9 km long (circumference) and accelerates protons from 14 GeV/c or 26 GeV/c to a momentum of up to 450 GeV/c. It is a cycling machine with cycles having a length of about 15 s. The transverse beam size is largest at injection and decreases with the square root of the beam energy during acceleration. For the operation as a synchrotron, the beam size is typically of the order of 1 mm.

When the SPS operates as LHC injector, up to 288 bunches are accelerated, each bunch with about $1.15\cdot10^{11}$ protons (nominal parameters). The bunch length is 0.5 ns and two neighboring bunches are separated by 25 ns so that the duration of the entire beam is 7.2 μs. The normalized emittance is $3.75\cdot10^{-6}$ m. Assuming a beta function of 100 m, the beam size is 0.88 mm. When the SPS was used as proton–antiproton collider, the luminosity was maximized by minimizing the beta function to 0.5 m. Assuming this value, the beam size would be as small as 0.06 mm.

The HiRadMat facility is dedicated to beam shock impact experiments. It is designed to allow testing of accelerator components, in particular those for LHC, to the impact of high-intensity pulsed beams. It has been constructed and commissioned during 2010–2011 [41–43]. Beam properties are shown in Table 1. It will provide a 440 GeV proton beam or a 36.9 TeV lead ion beam. For protons, the beam can allocate up to 288 bunches, each comprising of up to $1.7\cdot10^{11}$ particles. The focal size can go down to 0.1 mm σ_{rms}, thus providing a very dense beam (energy/size). The size can be tuned from 0.1 mm to 2 mm. The experimental area has a length of more than 9 m that allows up to three experiments to be installed in parallel.

Table 1
HiRadMat beam properties.

Parameter	Symbol	Protons	Pb ions
Particle energy	E	440 GeV	36.9 TeV
Bunch intensity	N_b	$1.7\cdot10^{11}$	$7\cdot10^{7}$
Max. number of bunches per pulse	n_{max}	288	52
Max. pulse intensity	$N_p = n_{max}\cdot N_b$	$4.9\cdot10^{13}$ protons	$3.64\cdot10^{9}$ ions
Bunch spacing	Δt_b	25 ns	100 ns
Min. beam size (rms)	σ_{beam}	0.1 mm	0.1 mm
RMS bunch length	σ_z	11.24 cm	11.24 cm
Pulse length	t_p	7.2 μs	5.2 μs

The primary purpose of the experiments suggested in this paper is to validate the existence of hydrodynamic tunneling that results from the hydrodynamic effects and to gain confidence with the methodology and simulation tools used. At later stages, other areas of research, for example, Warm Dense Matter (WDM) and HED physics may also benefit from this unique facility.

3. Simulations results

In this section we present the numerical simulations of the thermodynamic and hydrodynamic response of a solid copper cylindrical target that is facially impacted by the full SPS beam. The target length is 1.5 m and radius = 5 cm. Two focal spot sizes have been considered that are characterized by $\sigma = 0.5$ mm and 0.2 mm, respectively. These calculations have been done in two steps.

First, the energy deposition in the target from protons is calculated using the FLUKA code [44,45], assuming solid copper density (8.93 g/cm^3). This is a fully integrated particle physics and multi-purpose MonteCarlo simulation package capable of simulating all components of the particle cascades in matter up to TeV energies. FLUKA has many applications in high energy experimental physics and engineering, shielding, detector and telescope design, cosmic ray studies, dosimetry, medical physics and radiobiology as well as allows to simulate the interaction of beams with matter over a very wide energy range. The most relevant energy range for these applications being:

- Hadron and ion beams from as low as a few MeV/u up to 10,000 TeV/u
- Neutrons down to thermal energies
- Electromagnetic radiation from 1 keV up to 10,000 TeV
- Muons up to 10,000 TeV

Neutron transport and interactions below 20 MeV are treated using a coupled 72 neutron group – 22 gamma group library. Above 20 MeV for neutrons, and at all energies for the other particles, the time evolution of nuclear interactions in the models embedded in FLUKA is organized according to the following scheme:

- Glauber–Gribov cascade (not present below a few GeVs)
- (Generalized) Intranuclear cascade (GINC not present below 50 MeV)
- Pre-equilibrium emission
- Evaporation/fission/fragmentation
- Gamma de-excitation

Individual hadron–nucleon interactions, which are relevant as soon as the threshold for explicit GINC is passed, are described according to:

- Elastic and charge exchange scattering according to phase-shift analyses (up to few GeVs) and to eikonal models at higher energies
- Particle production according to resonance production and decay up to a few GeVs, and according to a quark-string model (DPM, Dual Parton Model) at higher energies

More details about the applied models and their performances as well as a vast amount of benchmarking can be found in Refs. [44,45]. It is to be noted that the models used in FLUKA also include nuclear size correction to the stopping power at very high energies.

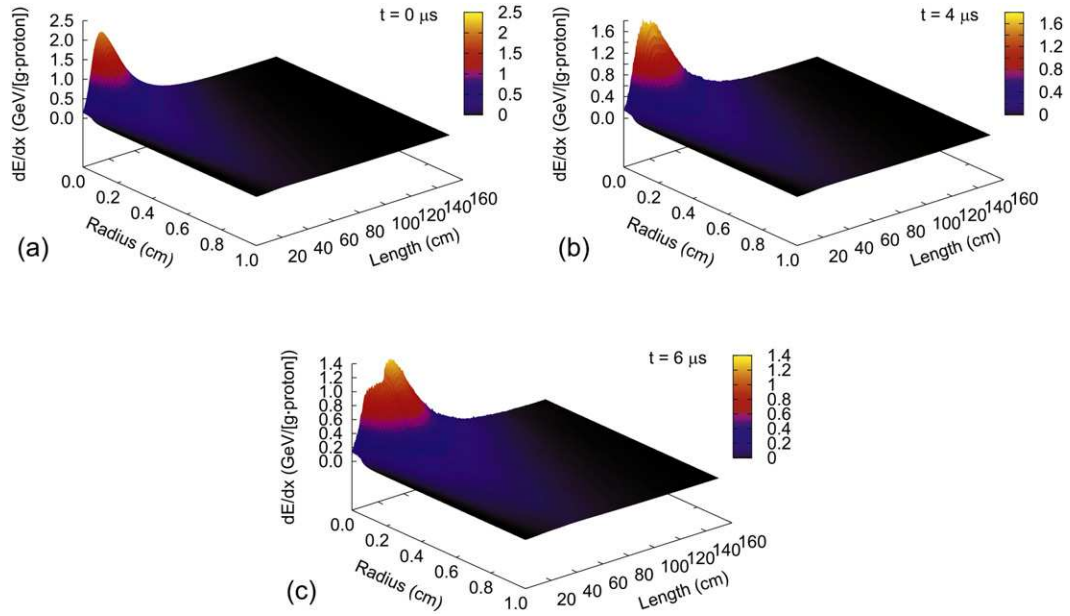

Fig. 1. Specific energy deposition per proton calculated by FLUKA code, proton energy 440 GeV, beam spot $\sigma = 0.5$ mm, copper target, radius = 5 cm, length = 1.5 m; (a) for solid density; (b) for the BIG2 density distribution at $t = 4$ μs and (c) for the BIG2 density distribution at $t = 6$ μs.

Second, this energy deposition data is used as input to a sophisticated two-dimensional hydrodynamic code, BIG2 [46] to calculate the beam–target interaction that causes hydrodynamic motion which leads to density reduction at the target center.

Multi-phase, multi-component semi-empirical Equation of State (EOS) data from Refs. [47,48] is used in BIG2 to model different physical states of copper in the calculations. The modified density distribution obtained from the BIG2 code is used back in the FLUKA code to calculate the corresponding modified energy deposition distribution for bunches arriving later. This new distribution is then used in the BIG2 code as the next step. In this manner, the two codes a run iteratively. The iteration interval is determined by the time during which the target density is reduced by 15–20% due to hydrodynamic effects.

3.1. Energy deposition calculations using FLUKA code

In the following are presented the energy deposition results that are obtained using the FLUKA code assuming two different focal spot sizes for the beam.

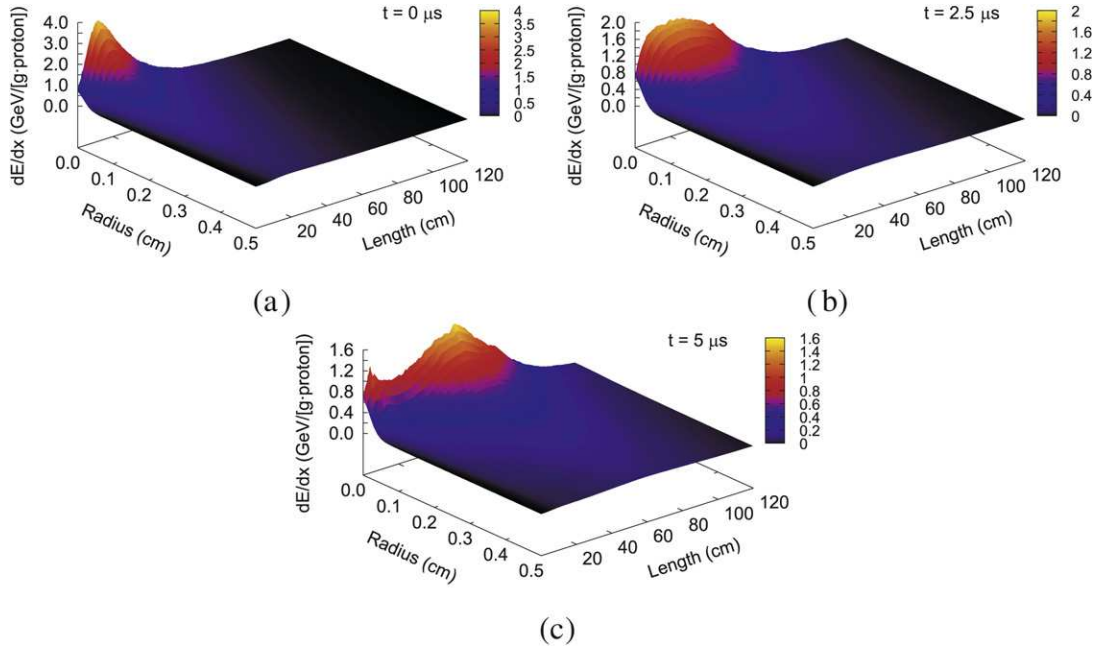

Fig. 2. Specific energy deposition per proton calculated by FLUKA code, proton energy 440 GeV, beam spot $\sigma = 0.2$ mm, copper target, radius = 5 cm, length = 1.5 m; (a) for solid density; (b) for the BIG2 density distribution at $t = 2.5$ μs and (c) for the BIG2 density distribution at $t = 5$ μs.

3.1.1. Case with $\sigma = 0.5$ mm

In this case an iteration step of 1 μs is used for interactive application of FLUKA and BIG2. In Fig. 1(a) we present the energy deposition per 440 GeV proton in units GeV/g as calculated by FLUKA assuming solid material density. This data shows that the range of the shower is about 75 cm in the target and the peak value of the distribution is around 2.1 GeV/p/g. The FLUKA calculations also suggest that approximately 36% beam energy escapes while 64% is absorbed in the target.

Fig. 1(b) presents the energy deposition obtained with the FLUKA code, but using the density distribution provided by BIG2 at $t = 4$ μs (fourth iteration). The energy deposition distribution has been modified with slight broadening of the energy peak.

The energy deposition plotted in Fig. 1(c) has been calculated by FLUKA using the density distribution obtained from BIG2 at $t = 6$ μs (sixth iteration). This figure shows that the energy peak has moved deeper into the target and the value of the energy peak has been reduced to 1.4 GeV/p/g.

3.1.2. Case with $\sigma = 0.2$ mm

A stronger beam focusing leads to higher specific energy deposition in the beam heated region that accelerates the hydrodynamic motion which requires that a shorter iteration step should be used. Therefore, in this case, we consider an iteration step of 500 ns for interactive application of FLUKA and BIG2.

In Fig. 2(a) we present the energy deposition per SPS proton in units GeV/g as calculated by FLUKA assuming solid material density. This figure shows that the range of the shower is about 90 cm in the target and the peak value of the distribution is around 4.0 GeV/p/g.

Fig. 2(b) presents the energy deposition obtained with the FLUKA code, but using the density distribution provided by BIG2 at $t = 2.5$ μs (fifth iteration). The energy deposition distribution has been strongly modified with substantial broadening of the energy peak. Moreover the maximum value of the peak has been reduced to 2 GeV/p/g.

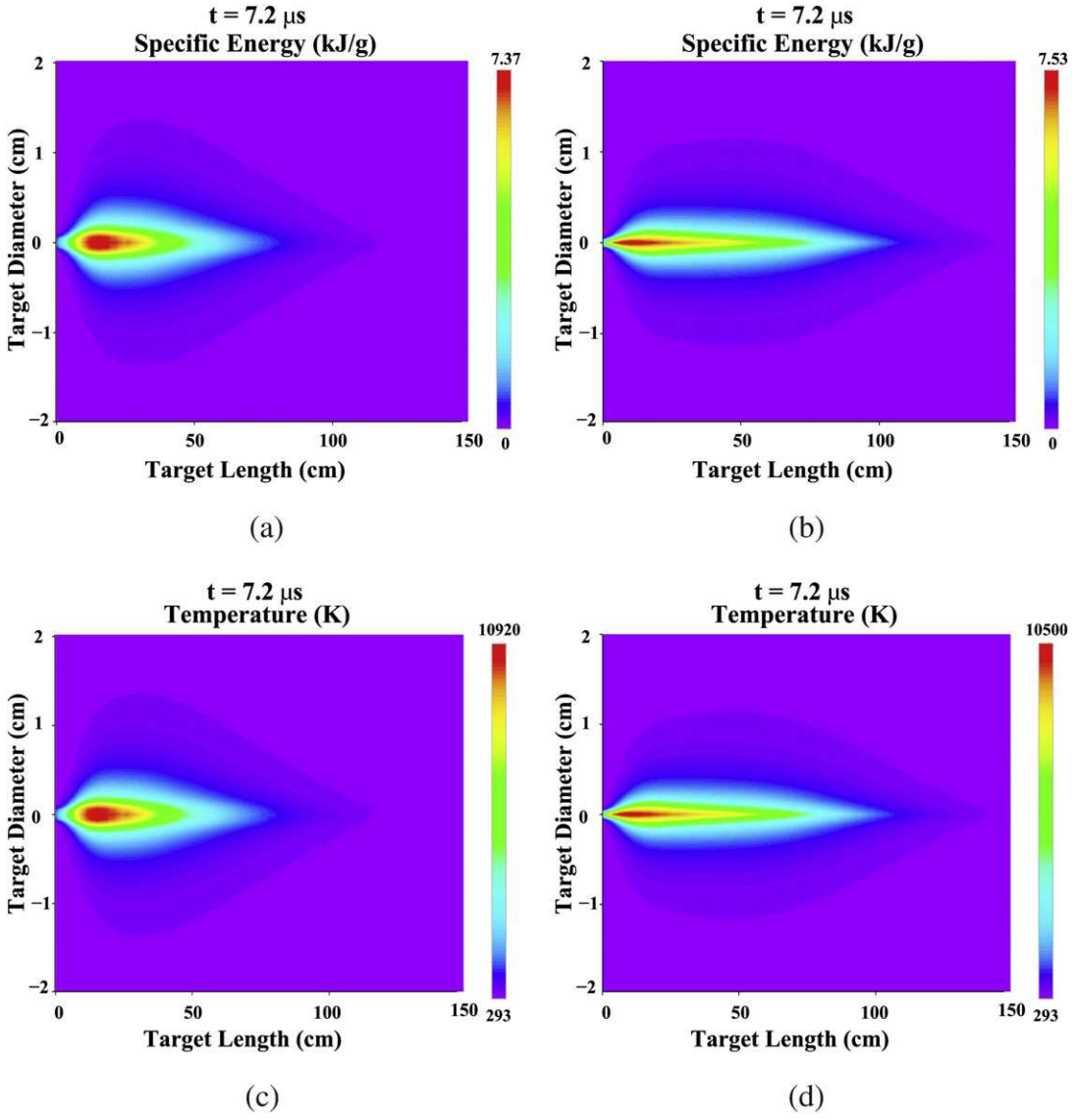

Fig. 3. Solid copper cylindrical target, $L = 1.5$ m, $r = 5$ cm, facially irradiated by 440 GeV SPS proton beam, 288 bunches, bunch intensity $= 1.15 \cdot 10^{11}$ protons, bunch length $= 0.5$ ns, bunch separation $= 25$ ns; (a) specific energy distribution at $t = 7.2$ μs (end of pulse) for $\sigma = 0.5$ mm; (b) specific energy distribution at $t = 7.2$ μs (end of pulse) for $\sigma = 0.2$ mm; (c) temperature distribution at $t = 7.2$ μs (end of pulse) for $\sigma = 0.5$ mm; (d) temperature distribution at $t = 7.2$ μs (end of pulse) for $\sigma = 0.2$ mm.

The energy deposition plotted in Fig. 2(c) has been calculated by FLUKA using the density distribution obtained from BIG2 at $t = 5$ μs (tenth iteration). This figure shows that the energy deposition has now two peaks. The main peak has moved much deeper into the target while the smaller peak lies at the beginning of the cylinder with a very low deposition region in between. This is due to the strong reduction in the target density in this middle region.

3.2. Hydrodynamic calculations using BIG2 code

In this section we present the hydrodynamic results obtained by using the BIG2 code for the two values of σ, respectively.

In Fig. 3(a) and (b), we present the specific energy deposition in the r–Z plane of the target at $t = 7.2$ μs (end of the beam) for $\sigma = 0.5$ mm and 0.2 mm, respectively. It is seen that the maximum specific energy deposition along the target axis is of the order of 7 kJ/g in both cases, but the shape of the distribution is very different. In the former case, the beam heated region is wider in the radial direction and shorter in the longitudinal direction as compared to the latter. This is in accordance with the geometrical conditions used in the two cases.

The corresponding temperature distributions are presented in Fig. 3(c) and (d), respectively. It is seen that in both cases the maximum target temperature at the end of the pulse is of the order of 10,000 K. This means that this part of the target will be severely damaged.

The pressure distributions corresponding to Fig. 4(a) and (b) are presented in Fig. 4(a) and (b), respectively. A maximum pressure of 2.28 GPa exists in the target at the end of the pulse (7.2 μs). The radial propagation of the pressure waves is also clearly seen in the two cases. It is also to be noted that by this time, the pressure wave has reached at the target surface in case of $\sigma = 0.5$ mm because of the larger size of the focal spot. In case of $\sigma = 0.2$ mm, on the other hand, the pressure wave has still not arrived at the cylinder surface, but has reached the opposite face of the cylinder due to the deeper penetration of the protons.

The target density distributions corresponding to the cases presented in Fig. 3(a) and (b) are shown in Fig. 4(c) and (d) respectively. It is seen in Fig. 4(c) that the minimum density along

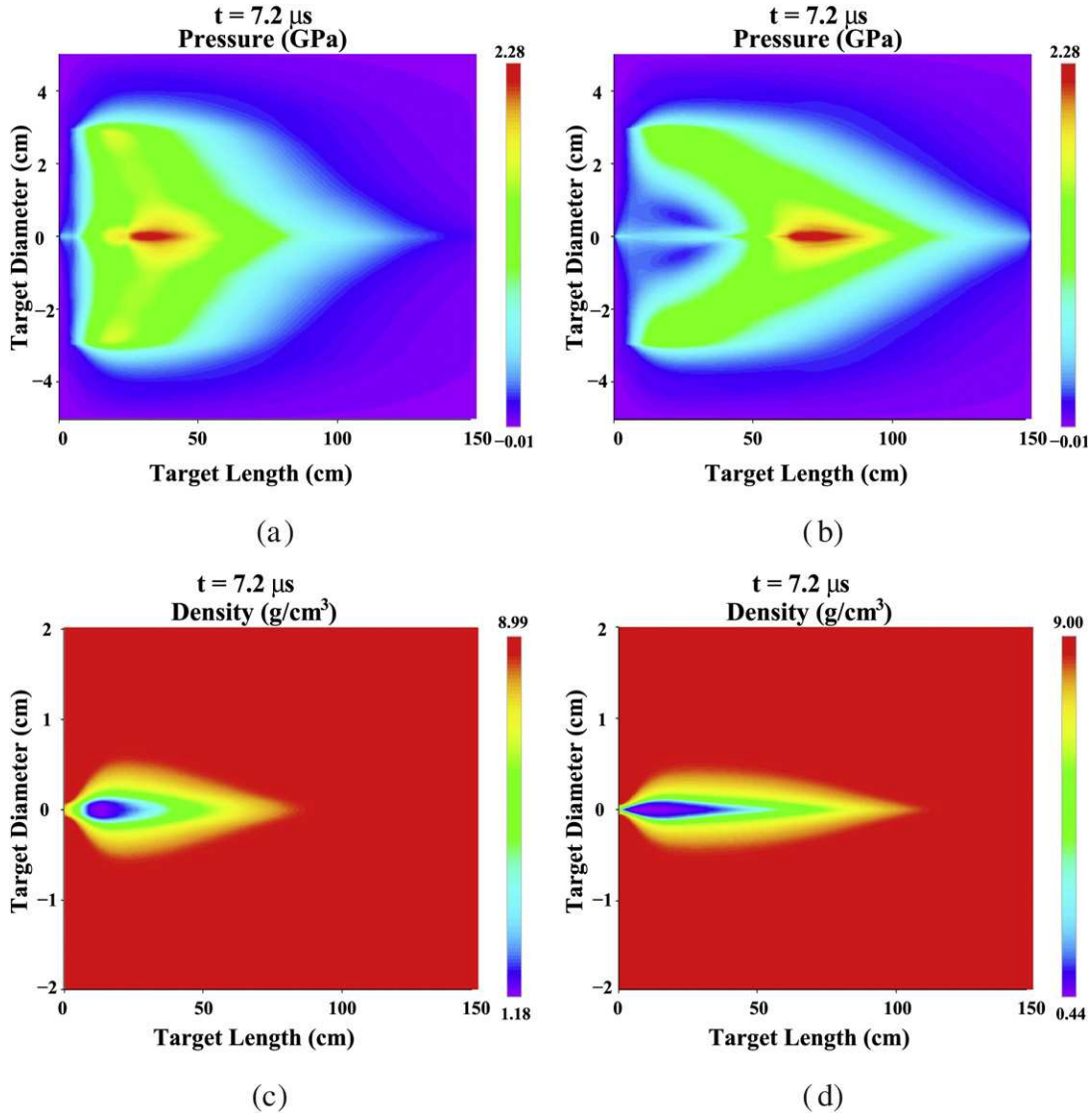

Fig. 4. Same target and beam parameters as in Fig. 3; (a) pressure distribution at $t = 7.2$ μs (end of pulse) for $\sigma = 0.5$ mm; (b) pressure distribution at $t = 7.2$ μs (end of pulse) for $\sigma = 0.2$ mm; (c) density distribution at $t = 7.2$ μs (end of pulse) for $\sigma = 0.5$ mm; (d) density distribution at $t = 7.2$ μs (end of pulse) for $\sigma = 0.2$ mm.

the target axis using $\sigma = 0.5$ mm is 1.18 g/cm^3 while Fig. 4(d) shows that in the case of $\sigma = 0.2$ mm, the minimum target density is 0.44 g/cm^3. It is well known that the physical conditions at the inner part of the target correspond to those of strongly coupled plasmas. Such plasmas are abundant in nature and are expected to be found in compact objects like brown dwarfs and Giant planets in our solar system and elsewhere.

In order to study this problem in a quantitative manner, we present the profiles of the specific energy deposition along the target axis at different times in Fig. 5(a) and (b) for $\sigma = 0.5$ mm and 0.2 mm, respectively. It is seen in Fig. 5(a) that the maximum value of the specific energy deposition at $t = 1$ μs is about 1.5 kJ/g that increases to 4 kJ/g at $t = 3$ μs. This value increases to 6 kJ/g at $t = 5$ μs and to about 7 kJ/g at $t = 7.2$ μs (end of the pulse). This shows that the specific energy density does not linearly increase with the number of bunches which can be explained in a simple manner. As the pressure in the absorption region increases, pressure waves are generated that move radially outwards and the density at the central part of the target is depleted. As a consequence, the subsequent bunches penetrate deeper into the target and the volume of the beam heated region increases with time which leads to the reduction in the rate of increase in the energy deposition. These effects are much more pronounced in Fig. 5(b) that corresponds to that case $\sigma = 0.2$ mm.

The temperature profiles corresponding to Fig. 5(a) and (b) are presented in Fig. 5(c) and (d) respectively. It is seen that the temperature profiles show the same behavior as the corresponding specific energy deposition profiles. It is seen that there is a flat part in every temperature cure in the two figures that represents the melting of the target. It is also interesting to note that this melting front moves in the longitudinal direction with time as the protons penetrate deeper into the target due to the hydrodynamic tunneling phenomenon.

The pressure profiles for the cases $\sigma = 0.5$ mm and 0.2 mm are presented in Fig. 6(a) and (b), respectively. It is interesting to note that unlike the temperature profiles, the behavior of the pressure profiles is opposite to that of the specific energy deposition profiles. It is seen in Fig. 6(a) that at $t = 1$ μs, the maximum pressure along the target axis is about 4.5 GPa that decreases significantly with time. This is due to the reduction in the target density in the beam heated region. Moreover the radially out-moving pressure waves shift the pressure peak away from the target center along the radius. These pressure waves are reflected at the target surface.

Fig. 6(b) shows that the pressure peak moves in the longitudinal direction as well. This is because of the faster and deeper hydrodynamic tunneling of the protons and the shower in this case.

The density profiles along the target axis at different times corresponding to the cases $\sigma = 0.5$ mm and 0.2 mm, are presented in Fig. 6(c) and (d) respectively. It is seen the density depletion front moves towards the right with constant speeds in both cases. At the end of the pulse a large part of the target in the beam heated region is converted to a high density (few % of the solid density) and low temperature strongly coupled plasma.

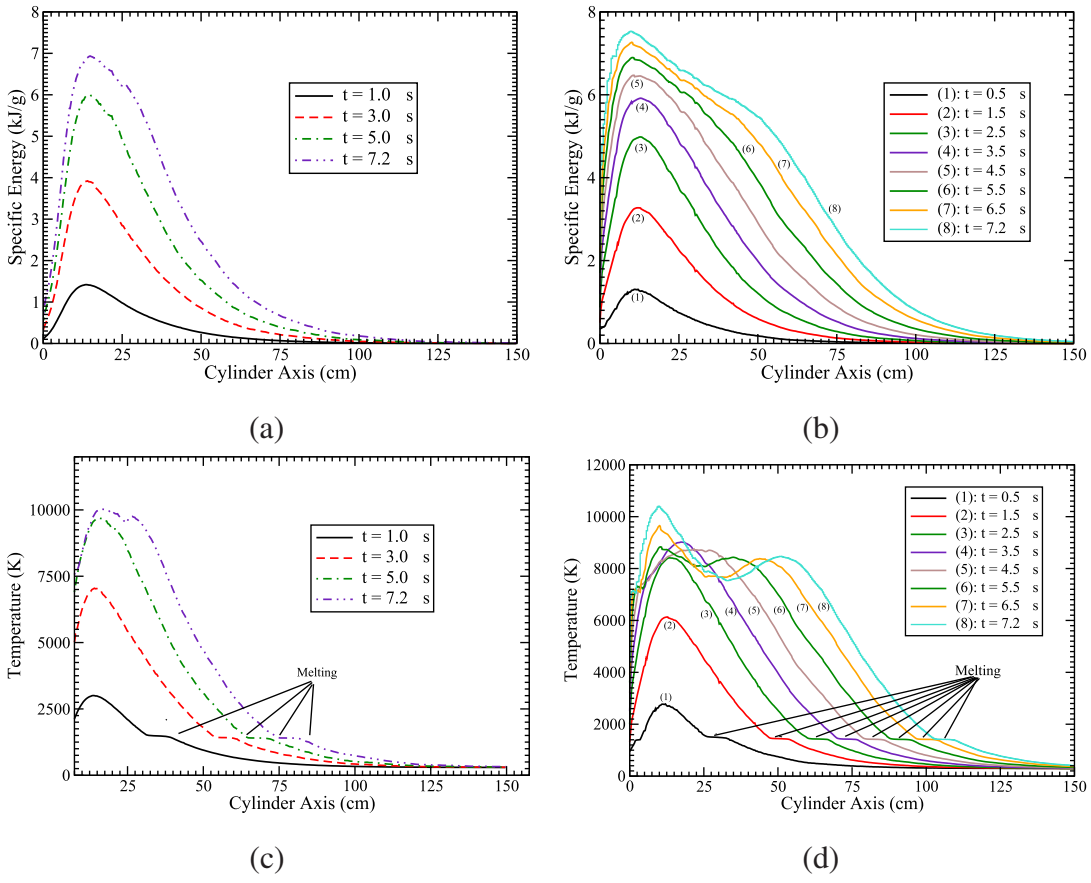

Fig. 5. Profiles of physical parameters along the cylinder axis at different times; (a) specific energy deposition for $\sigma = 0.5$ mm; (b) specific energy deposition for $\sigma = 0.2$ mm; (c) temperature for $\sigma = 0.5$ mm; (d) temperature for $\sigma = 0.2$ mm.

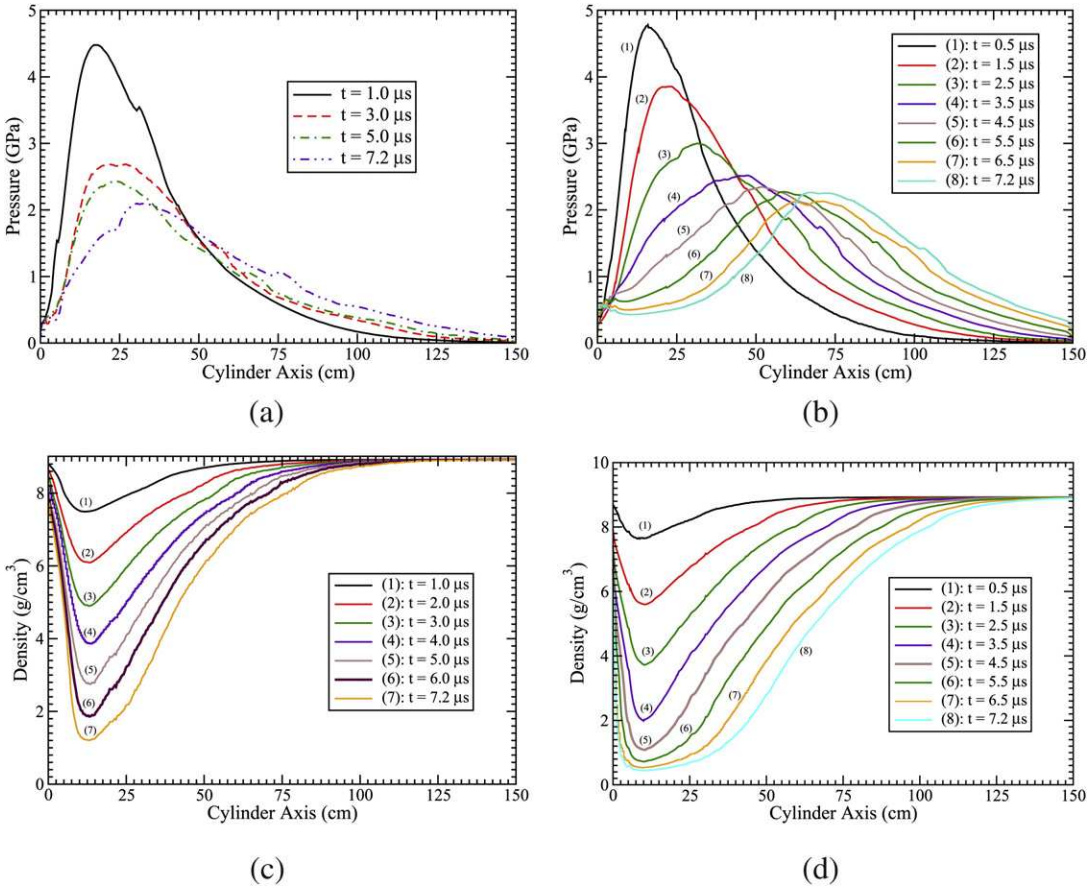

Fig. 6. Profiles of physical parameters along the cylinder axis at different times; (a) pressure for $\sigma = 0.5$ mm; (b) pressure for $\sigma = 0.2$ mm; (c) density for $\sigma = 0.5$ mm; (d) density for $\sigma = 0.2$ mm.

4. Conclusions

The HiRadMat at CERN is a unique experimental facility where an intense proton beam is available for beam–target heating experiments. Numerical simulations presented in this paper show that the SPS beam has great potential to generate large samples of HED matter including the WDM and strongly coupled plasmas. Particle beams have numerous advantages over traditional drivers that are used to produce HED matter in the laboratory. It is therefore highly desirable to study this venerable area of research at this facility. Specific experiments to study different problems related to the HED physics are currently being designed and may be carried out at the HiRadMat facility in the future.

References

[1] N.A. Tahir, K.A. Long, Phys. Lett. A 90 (1982) 242.
[2] K.A. Long, N.A. Tahir, Phys. Lett. A 91 (1982) 451.
[3] N.A. Tahir, K.A. Long, Laser Part. Beams 2 (1984) 371.
[4] N.A. Tahir, K.A. Long, Z. Phys. A 325 (1986) 99.
[5] K.A. Long, N.A. Tahir, Nucl. Fusion 26 (1986) 555.
[6] R.O. Bangerter, J.W.K. Mark, A.R. Thiessen, Phys. Lett. A 90 (1982) 225.
[7] A.R. Piriz, Phys. Fluids 31 (1988) 658.
[8] A.R. Piriz, M.M. Sanchez, Phys. Plasmas 5 (1998) 2721.
[9] C. Deutsch, Ann. Phys. (Paris) 11 (1986) 1.
[10] B.G. Logan, L.J. Perkins, J.J. Barnard, Phys. Plasmas 15 (2008) 072701.
[11] N.A. Tahir, D.H.H. Hoffmann, J.A. Maruhn, K.-J. Lutz, R. Bock, Phys. Plasmas 5 (1998) 4426.
[12] N.A. Tahir, D.H.H. Hoffmann, J.A. Maruhn, P. Spiller, R. Bock, Phys. Rev. E 60 (1999) 4715.
[13] N.A. Tahir, D.H.H. Hoffmann, A. Kozyreva, A. Shutov, J.A. Maruhn, U. Neuner, A. Tauschwitz, P. Spiller, R. Bock, Phys. Rev. E 61 (2000) 1975.
[14] N.A. Tahir, D.H.H. Hoffmann, A. Kozyreva, A. Tauschwitz, A. Shutov, J.A. Maruhn, P. Spiller, U. Neuner, J. Jacoby, M. Roth, R. Bock, H. Juranek, R. Redmer, Phys. Rev. E 63 (2001) 016402.
[15] N.A. Tahir, A. Kozyreva, P. Spiller, D.H.H. Hoffmann, A. Shutov, Phys. Rev. E 63 (2001) 036407.
[16] N.A. Tahir, A. Shutov, D. Varentsov, P. Spiller, S. Udrea, D.H.H. Hoffmann, I.V. Lomonosov, J. Wieser, M. .Kirk, A.R. Piriz, V.E. Fortov, R. Bock, Phys. Rev. Spec. Top. Accel. Beams 6 (2003) 020101.
[17] N.A. Tahir, H. Juranek, A. Shutov, R. Redmer, A.R. Piriz, M. Temporal, D. Varentsov, S. Udrea, D.H.H. Hoffmann, C. Deutsch, I.V. Lomonosov, V.E. Fortov, Phys. Rev. B 67 (2003) 184101.
[18] N.A. Tahir, B. Goddard, V. Kain, R. Schmidt, A. Shutov, I.V. Lomonosov, A.R. Piriz, M. .Temporal, D.H.H. Hoffmann, V.E. Fortov, J. Appl. Phys. 97 (2005) 083532.
[19] N.A. Tahir, V. Kain, R. Schmidt, A. Shutov, I.V. Lomonosov, V. Gryaznov, A.R. Piriz, M. Temporal, D.H.H. Hoffmann, V.E. Forotv, Phys. Rev. Lett. 94 (2005) 135004.
[20] N.A. Tahir, C. Deutsch, V.E. Fortov, V. Gryaznov, D.H.H. Hoffmann, M. Kulish, I.V. Lomonosov, V. Mintsev, P. Ni, D. Nikolaev, A.R. Piriz, N. Shilkin, P. Spiller, A. Shutov, M. Temporal, V. Ternovoi, S. Udrea, D. Varentsov, Phys. Rev. Lett. 95 (2005) 035001.
[21] N.A. Tahir, P. Spiller, S. Udrea, O.D. Cortazar, C. Deutsch, V.E. Fortov, V. Gryaznov, D.H.H. Hoffmann, I.V. Lomonosov, P. Ni, A.R. Piriz, A. Shutov, M. Temporal, D. Varentsov, Nucl. Instrum. Meth. B 245 (2006) 85.
[22] N.A. Tahir, R. Schmidt, M. Brugger, R. Assmann, A. Shutov, I.V. Lomonosov, V. Gryaznov, A.R. Piriz, S. Udrea, D.H.H. Hoffmann, et al., Phys. Plasmas 16 (2009) 082703.
[23] N.A. Tahir, Th. Stöhlker, A. Shutov, I.V. Lomonosov, V.E. Fortov, M. French, N. Nettelmann, R. Redmer, A.R. Piriz, C. Deutsch, et al., New J. Phys. 12 (2010) 073022.
[24] N.A. Tahir, A. Shutov, A.P. Zharkov, A.R. Piriz, Th. Stöhlker, Phys. Plasmas 15 (2011) 051003.
[25] A.R. Piritz, J.J. Lopez Cela, M.C. Serna Moreno, N.A. Tahir, D.H.H. Hoffmann, Laser Part. Beams 24 (2006) 275.
[26] S.A. Piriz, A.R. Piriz, N.A. Tahir, Phys. Plasmas 16 (2009) 082706.
[27] U. Neuner, R. Bock, M. Roth, P. Spiller, C. Constantin, U.N. Funk, M. Geissel, S. Hakuli, D.H.H. Hoffmann, J. Jacoby, A. Kozereva, N.A. Tahir, S. Udrea, D. Varentsov, A. Tauschwitz, Phys. Rev. Lett. 85 (2000) 4518.

[28] U.N. Funk, R. Bock, M. Dornik, M. Geissel, M. Stetter, S. Stöwe, N.A. Tahir, D.H.H. Hoffmann, Nucl. Instrum. Meth. A 415 (1998) 68.
[29] S. Udrea, V. Ternovoi, N. Shilkin, A. Fertman, V.E. Fortov, D.H.H. Hoffmann, A. Hug, M.I. Kulish, V. Mintsev, P. Ni, D. Nikolaev, N.A. Tahir, V. Turtikov, D. Varentsov, D. Yuriev, Nucl. Instrum. Meth. A 577 (2007) 257.
[30] J.J. Barnard, J. Armijo, R.M. More, A. Friedman, I. Kaganovich, B.G. Logan, M.M. Marinak, G.E. Penn, A.B. Sefkow, P. Santhanam, et al., Nucl. Instrum. Meth. A 577 (2007) 275.
[31] P. Ni, D.H.H. Hoffmann, M. Kulish, D. Nikolaev, N.A. Tahir, S. Udrea, D. Varentsov, H. Wahl, J. Phys. IV France 133 (2006) 977.
[32] S.F. Ng, J.J. Barnard, P.T. Leung, S.S. Yu, High Energy Density Phys. 7 (2011) 203.
[33] J. Armijo, J.J. Barnard, Phys. Rev. E 83 (2011) 051507.
[34] N.A. Tahir, R. Schmidt, A. Shutov, I.V. Lomonosov, A.R. Piriz, D.H.H. Hoffmann, C. Deutsch, V.E. Fortov, Phys. Rev. E 79 (2009) 046410.
[35] N.A. Tahir, J. Blanco Sancho, A. Shutov, R. Schmidt, A.R. Piriz, Phys. Rev. Spec. Top. Accel. Beams 18 (2012) 032704.
[36] N. Mokhov, T. Murphy, M. Palmer, T. Toohig, F. Turkot, A. Vanginneken, Bull. Am. Phys. Soc. (1981).
[37] N.A. Tahir, V. Kim, I.V. Lomonosov, D.A. Grigoriev, A.R. Piriz, H. Weick, H. Geissel, D.H.H. Hoffmann, Laser Part. Beams 25 (2007) 295.
[38] N.A. Tahir, R. Schmidt, M. Brugger, R. Assmann, A.V. Shutov, I.V. Lomonosov, A.R. Piriz, D.H.H. Hoffmann, C. Deutsch, V.,E. Fortov, New J. Phys. 10 (2008) 073028.
[39] N.A. Tahir, R. Schmidt, M. Brugger, R. Assmann, A. Shutov, I.V. Lomonosov, V.E. Fortov, A.R. Piriz, C. Deutsch, D.H.H. Hoffmann, Nucl. Instrum. Meth. A 606 (2009) 186.
[40] J. Blanco Sancho, F. Burkart, N. Charitonidis, I. Efthymiopoulos, D. Grenier, C. Maglioni, R. Schmidt, C. Theis, D. Wollmann, N.A. Tahir, in: Proceedings of HB 2012, Beijing, China, 2012.
[41] C. Hessler, M. Arruat, J. Bauche, K. Bestmann, J. Blanco, N. Conan, K. Cornelis, I. Efthymiopoulos, H. Gaillard, B. Goddard, et al., in: Proceedings of the IPAC'10 Conference, San Sebastian, 2011 (IPAC'11/EPS-AG) (2011).
[42] J. Blanco Sancho, N. Conan, K. Cornelis, B. Goddard, C. Hessler, L. Jensen, V. Kain, M. Meddahi, C. Theis, P. Vojtyla, J. Wenninger, HiRadMat Low Intensity Beam Commissioning (Jul 2011). CERN-ATS-Note-2011-126 PERF.
[43] J. Blanco Sancho, N. Conan, K. Cornelis, B. Goddard, C. Hessler, L. Jensen, V. Kain, M. Meddahi, C. Theis, H. Vincke, P. Vojtyla, J. Wenninger, HiRadMat High Intensity Beam Commissioning (Nov 2011). CERN-ATS-Note-2011-56 PERF.
[44] A. Fasso, A. Ferrari, J. Ranft, P.R. Sala, Tech. Rep., CERN, 2005.
[45] A. Fasso, A. Ferrari, S. Roesler, R.P. Sala, G. Battistoni, F. Cerutti, E. Gadioli, M.V. Garzelli, F. Ballarini, A. Ottolenghi, A. Empl, J. Ranft, in: Conference on Computing in High Energy and Nuclear Physics, La Jolla, USA, 2003.
[46] V.E. Fortov, B. Goel, C.D. Munz, A.L. Ni, A. Shutov, O.V. Vorobiev, Nucl. Sci. Eng. 123 (1996) 169.
[47] I.V. Lomonosov, Laser Part. Beams 25 (2007) 567.
[48] I.V. Lomonosov, N.A. Tahir, Appl. Phys. Lett. 92 (2008) 101905.